Review

4-D noise-based seismology at volcanoes: Ongoing efforts and perspectives

Florent Brenguier [a,*], Diane Rivet [b], Anne Obermann [c], Nori Nakata [d], Pierre Boué [a], Thomas Lecocq [e], Michel Campillo [a], Nikolai Shapiro [f]

[a] ISTerre - University of Grenoble Alpes - CNRS, France
[b] Géoazur - Université Nice Sophia Antipolis - CNRS, France
[c] Swiss Seismological Service, ETH, Switzerland
[d] Standford University, United States
[e] Royal Observatory of Belgium, Belgium
[f] Institut de Physique du Globe de Paris - CNRS, France

ARTICLE INFO

ABSTRACT

Monitoring magma pressure buildup at depth and transport to surface is a key point for improving volcanic eruption prediction. Seismic waves, through their velocity dependence to stress perturbations, can provide crucial information on the temporal evolution of the mechanical properties of volcanic edifices. In this article, we review past and ongoing efforts for extracting accurate information of temporal changes of seismic velocities at volcanoes continuously in time using records of ambient seismic noise. We will first introduce the general methodology for retrieving accurate seismic velocity changes from seismic noise records and discuss the origin of seismic velocity temporal changes in rocks. We will then discuss in a second part how noise-based monitoring can improve our knowledge about magmatic activity at a long (years) to a short (days) time scale taking example from Piton de la Fournaise volcano (La Réunion). We will also mention ongoing efforts for operational noise-based seismic monitoring on volcanoes. Further, we will discuss perspectives for improving the spatial localization of detected velocity changes at depth with a special focus on the use of dense seismic arrays. In the last part, we will finally explore the complex response of volcanic regions to seismic shaking with an example from Japan and show how imaging seismic velocity susceptibility allows characterizing the state of pressurized fluids in volcanic regions.

© 2016 Elsevier B.V. All rights reserved.

Contents

* Corresponding author.

1. Introduction

Volcanic eruptions are among the most dramatic manifestations of Earth's activity. Geological, geophysical and geochemical studies provide accurate insights into where on Earth volcanic and tectonic activity focuses and aim at characterizing the properties of systems that lead to catastrophic events. As an example, on volcanic systems, low seismic velocities and high Vp/Vs ratio delineate regions with magma and/or rocks with pressurized gas-filled pores (Husen et al., 2004; Lees, 2007; Jaxybulatov et al., 2014). These observations serve as inputs for models of the long-term behavior of volcanic systems that help for example to predict the frequency and magnitude of super-eruptions (Caricchi et al., 2014). Imaging tectonic and volcanic hazardous regions thus provides a background for understanding the origin of catastrophic events (Koulakov, 2013). On the other hand improving hazard assessment requires catching the temporal evolution of these active volcanic systems at a mid- to short time scale (from years to hours).

In the volcanic domain, the transport of magma to the surface, which ultimately may lead to eruptions, is caused by pressure buildup at depth induced by the deep supply of magma and volcanic fluid pressurization (Chang et al., 2007). This short-term (months to hours) magma pressurization and transport through the brittle upper-crust and volcanic edifice to surface before eruptions can be monitored through deformation and seismicity observations to provide a useful indicator for upcoming eruptions (Cayol et al., 2000; Taisne et al., 2011). Seismic waves, through their velocity dependence to stress perturbations, can also provide crucial information on the temporal evolution of the mechanical properties of volcanic edifices (Ratdomopurbo and Poupinet,

1995; Gerst and Savage, 2004). Significant progress has been made in 4-D tomography (3D + time) based on picking P and S-wave arrival times of earthquakes but the precision of such approaches is still of the order of percents in temporal changes of seismic velocities and at best months in terms of temporal resolution (Patanè et al., 2006). Such approaches will unlikely be able to reach the level of precision required to detect small stress changes at depth prior to eruptions (e.g. kilo Pascal stress changes associated with daily to monthly velocity changes of the order of 0.01%). On the other hand, a significant effort in active source monitoring has led Japanese groups to develop a continuously vibrating source (ACROSS, Ikuta et al., 2002) for the purpose of monitoring active faults and volcanoes. Up to now no significant results have been reported from this approach, which suffers from the very sparse spatial sampling of the monitored areas.

The Earth is not static but permanently vibrating even when no strong energetic sources of vibration occur (e.g. earthquakes or volcanic eruptions). These background vibrations of amplitude of the order of micro-meters of particle displacement arise from the interactions between the solid Earth and its envelope at very long period of few hundreds of seconds (seismic hum, Rhie and Romanowicz, 2004), at periods around 10 s (microseisms, Kedar and Webb, 2005) and at shorter periods below 1 s (e.g. effects of winds, Hillers and Ben-Zion, 2011). At high frequencies, seismic noise has also a strong anthropogenic origin (Hillers et al., 2014). In the following we will describe how we can benefit from this perpetual motion of the vibrating Earth's crust to monitor time-lapse changes of the mechanical properties of rocks in regions of active tectonic and volcanic activity (4-D imaging).
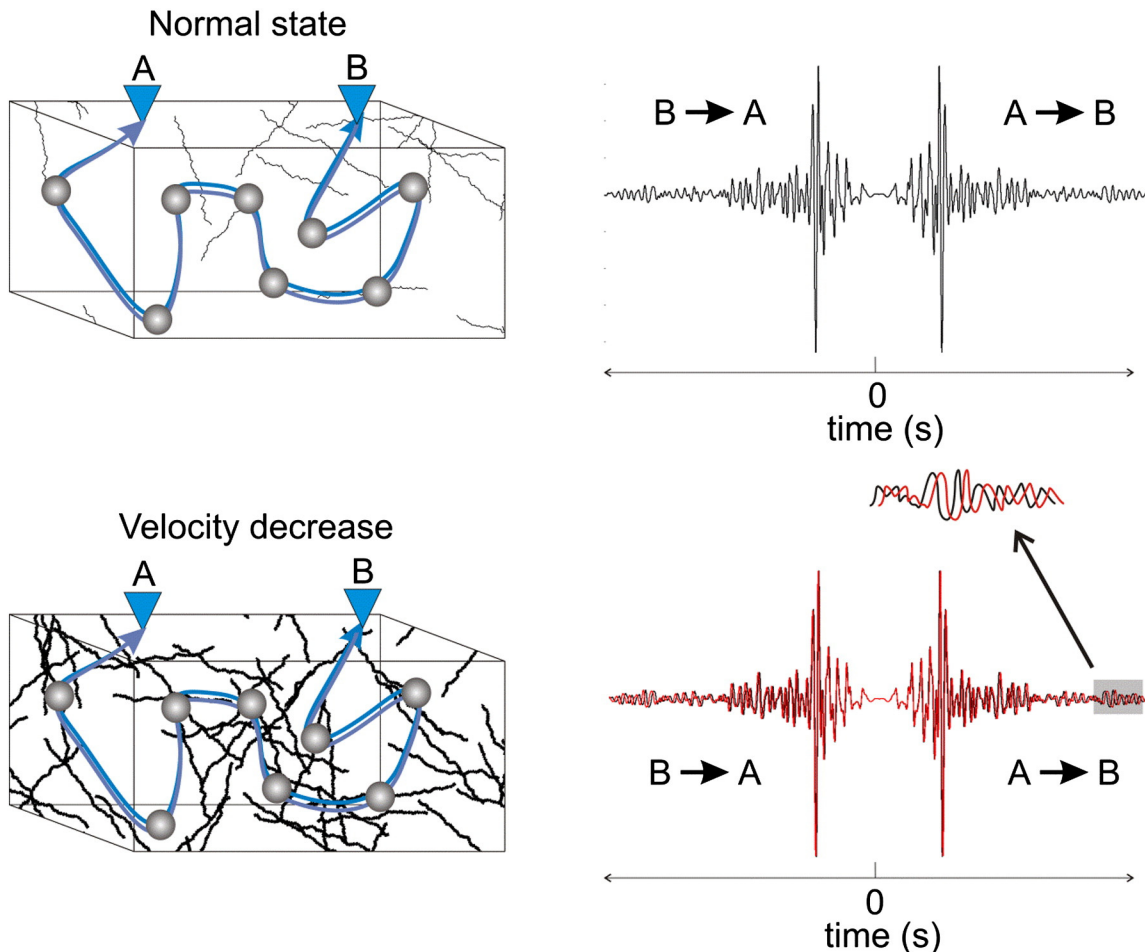
Fig. 1. Sketch representing the principle of seismic velocity change detection from travel time perturbations in the coda of noise correlation functions. (For interpretation of the references to color in this figure, the reader is referred to the web version of this article.)
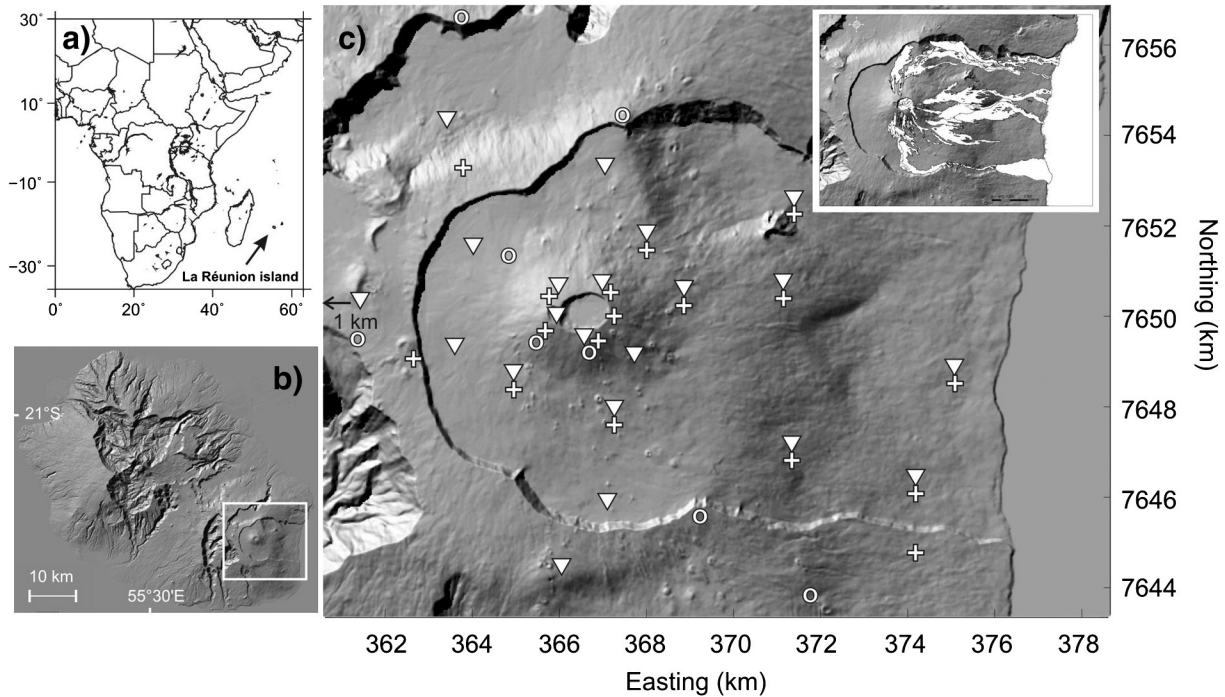
Fig. 2. Location of a) La Réunion island, b) Piton de la Fournaise volcano (white rectangle) and c) the UnderVolc and Observatory seismic and GPS networks. UnderVolc broad-band seismic stations are shown as inverted triangles, GPS as crosses and observatory short-period seismic stations as circles. The inset map shows lava flows from 2000 to 2010 (courtesy of OVPF, T. Staudacher, Z. Servadio).

We will first introduce the general methodology for retrieving accurate seismic velocity changes from seismic noise records and discuss the origin of seismic velocity temporal changes in rocks. We will then discuss in a second part how noise-based monitoring can improve our knowledge about magmatic activity at a long (years) to a short (days) time scale taking examples from Piton de la Fournaise volcano (La Réunion). We will also mention ongoing efforts for operational noise-based seismic monitoring on volcanoes. Further, we will discuss perspectives for improving the spatial localization of detected velocity changes at depth with a special focus on the use of dense seismic arrays. In the last part, we will finally explore the complex response of volcanic regions to seismic shaking with an example from Japan and show how imaging seismic velocity susceptibility allows characterizing the state of pressurized fluids in volcanic regions.

2. Noise-based seismology

In a pioneering work, Aki (1957) described how the spatial correlation of the ambient seismic noise recorded at different sensors could be used to assess the seismic velocity field below the deployed array. He was thus the first to propose the idea of extracting useful information on the subsurface from an apparent stochastic noise seismic wavefield. A breakthrough result came from Lobkis and Weaver (2001) who showed that the correlation function of a diffuse acoustic field between two sensors is proportional to the Green's function of the medium between these two sensors. This approach was further theoretically explored by Campillo (2006). In seismology the first convincing realization of this idea was obtained by Campillo and Paul (2003) who used the coda of earthquakes as a diffuse field to correlate for Green's function reconstruction at a regional scale. Shapiro and Campillo (2004) obtained similar results using ambient microseismic noise initiating numerous applications of this approach for imaging the crust at a regional scale (e.g. Shapiro et al., 2005) as well as volcanoes (Brenguier et al., 2007). These results revolutionized seismological studies that were essentially based on the analysis of discrete in time earthquake records. Our ability to extract useful information from ambient seismic

noise arose at the same time as the discovery of nonvolcanic tremors and slow earthquakes and led seismologists to consider continuous seismic records with great interest. Now, almost every seismic network in the world records data continuously in time allowing for future discoveries.

Taking advantage of continuous seismic records, Sens-Schönfelder and Wegler (2006) were the first to propose the consideration of daily cross-correlations of noise as repetitive in time Green's functions, which can be used to assess seismic velocity temporal changes. The breakthrough result was that, using continuous time series of ambient noise, it is possible to continuously measure time-lapse changes of the subsurface mechanical properties. This approach thus allows circumventing the traditional sparse temporal resolution of monitoring observations based on repeating seismic events (Poupinet et al., 1984).

In order to measure accurate seismic velocity changes, Sens-Schönfelder and Wegler (2006) proposed to apply an approach described initially by Poupinet et al. (1984) and later referred to as coda wave interferometry (Snieder et al., 2002; Snieder and Hagerty, 2004; Grêt et al., 2005; Wegler et al., 2006). The principle is summarized in Fig. 1. The top right seismogram represents the symmetric causal and acausal Green's functions reconstructed from noise correlation. The top left figure represents the travel paths of late coda arrivals that originate from scattering in the complex medium. If the medium experiences a stress perturbation that results in an homogeneous, isotropic seismic velocity decrease $\left(\delta v / v\right)$ of compressional and shear waves (lower part of the figure), then the travel time perturbations of the direct and coda arrivals ($\delta \tau$, see red seismogram) in reference to the normal state are linearly proportional to their travel times (τ). Moreover, the relative travel time perturbation $\left(\delta \tau / \tau\right)$ is equal to the opposite of the medium relative seismic velocity change between the normal and the perturbed state $\left(\delta \tau / \tau = -\delta v / v\right)$ for small δv. By measuring travel time perturbations along the coda of the noise correlation functions, it is thus possible to assess the relative velocity change in the medium (Sens-Schönfelder and Wegler, 2006; Brenguier et al., 2008a; Brenguier et al., 2008b).
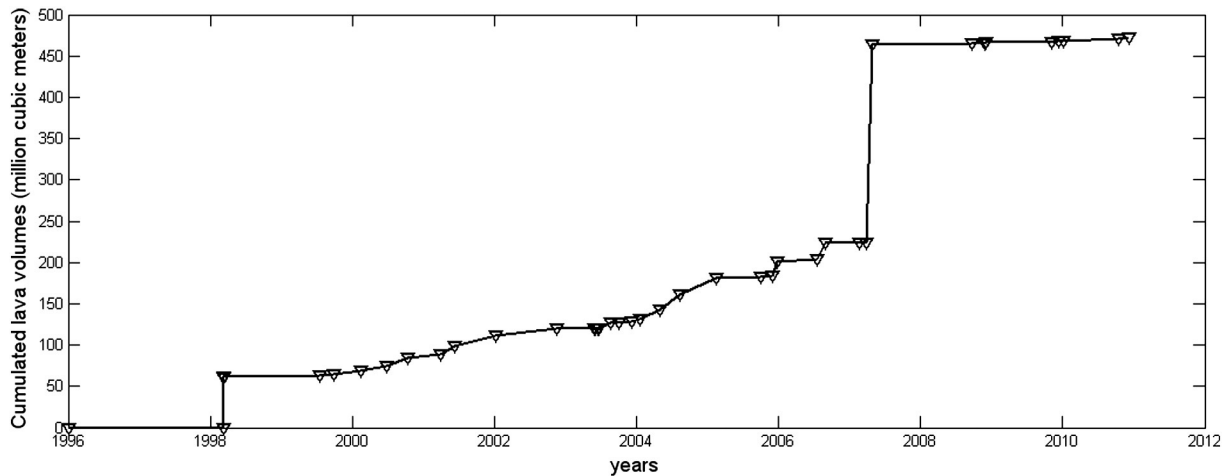
Fig. 3. Cumulative emitted lava volumes since the 1998 eruption. Each triangle represents the occurrence of a volcanic eruption of PdF.

One of the most important limitations of noise-based monitoring is that it requires stable sources in time. Hadziioannou et al. (2009) studied in a laboratory experiment the relation between the amount of stable sources and the errors on monitored seismic velocity changes in a rock sample. From a theoretical point of view, Weaver et al. (2011) and Colombi et al. (2014) proposed a formulation to estimate the uncertainty of passively derived velocity changes taking into account changes in the noise source properties. Clarke et al. (2011) proposed a numerical study to assess the accuracy of velocity change estimates from noise correlations proposing a relation between the resolution of velocity changes and the signal-to-noise ratio of the noise cross-correlations. Sources of the background seismic signals on active volcanoes might change in time. During quiet periods, the continuous seismic records are dominated by the ambient seismic noise, as elsewhere. During the periods of the increased activity, the volcanoes can themselves become sources of strong seismic tremors. These tremors might significantly modify the content of the inter-station cross-correlations (Ballmer et al., 2013; Droznin et al., 2015). Therefore, the stability of the cross-correlations needs to be checked with a particular attention when monitoring active volcanoes. Here, we see that the accuracy of velocity change estimates from noise correlations is hampered by the actual coherence between consecutive correlations. Different authors proposed approaches to increase the coherence between a set of correlation functions. Among those, Baig et al. (2009) were able to improve by a factor of 2 the precision of velocity change measurements on Piton de la Fournaise volcano using a phase coherence filter (Schimmel and Gallart, 2007) of noise correlations allowing for a precise detection of precursory velocity changes to eruptions.

Overall, it is important to point out from previous works that the accuracy of seismic velocity temporal change measurements from noise correlations can reach 10^{-5} which means for example detecting a velocity change of 0.02 m/s over a medium of average velocity 2000 m/s. This very high level of accuracy is similar to the one obtained with active repeating sources (Yamamura et al., 2003). However, passive monitoring is currently less accurate to locate changes in space compared to active source monitoring because it relies on coda-wave interferometry rather than on direct body-waves (see the perspective section on Localization).
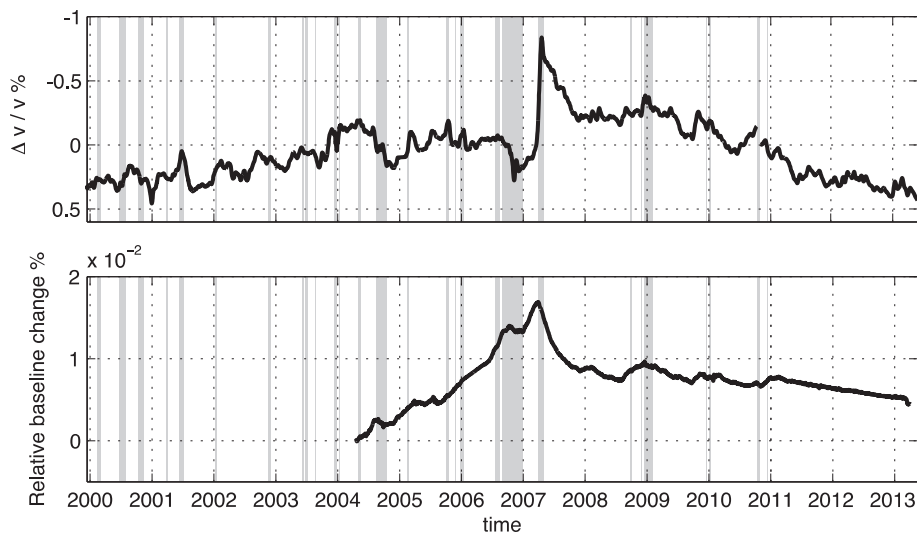
Fig. 4. Seismic velocity changes averaged over the edifice from surface to a few kilometer depth (top) and GPS-derived baseline change averaged over the central part of the edifice and corrected for the co-eruptive displacement due to dyke emplacement (bottom, see Rivet et al. (2014) for details). Eruptive periods are marked as gray boxes.
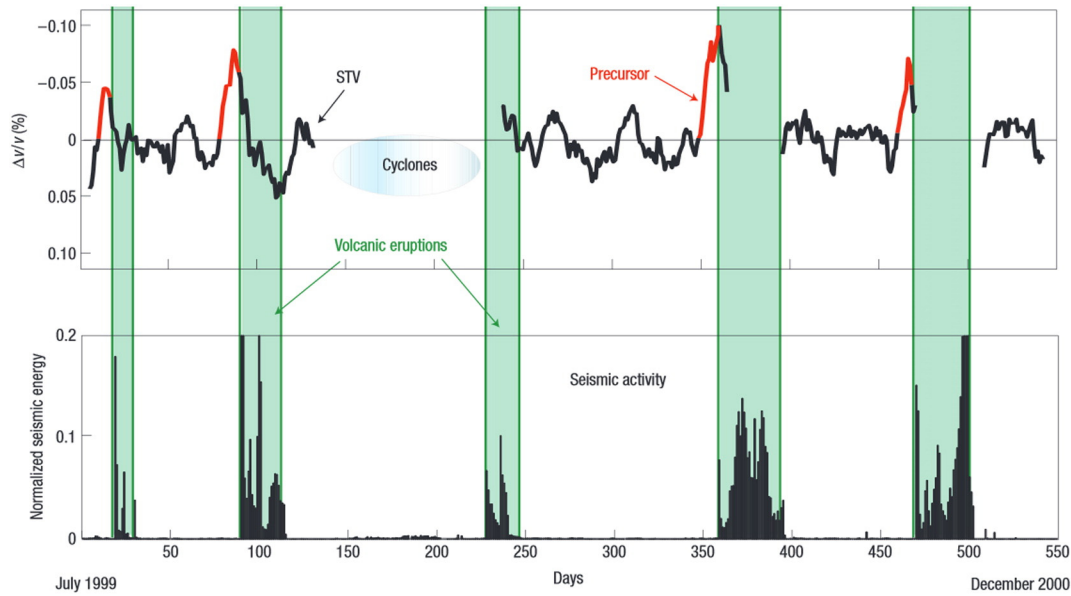
Fig. 5. Seismic velocity reductions preceding eruptions on PdF volcano versus seismic energy which is computed as the daily averaged RMS value of continuous seismic signals recorded at PdF. Green boxes show the periods of eruptions (Brenguier et al., 2008a). (For interpretation of the references to color in this figure legend, the reader is referred to the web version of this article.)

3. The seismic velocity dependence to stress and damage changes

The ordinary theory of elasticity is limited to infinitesimal deformation of perfectly elastic solids where strain is linearly proportional to stress and seismic velocities are not dependant on stress. It has been observed for decades that the seismic velocities of rocks increase with increasing confining pressure (Birch, 1966). This behavior of solids has been described in detail from a theoretical elasticity model of finite deformation (Hughes and Kelly, 1953; Egle and Bray, 1976). The stress dependence of elastic moduli of rocks has also been investigated in the light of poro-elastic theory (O'Connell and Budiansky, 1974) which relates seismic velocity changes to crack density, fluid saturation and fluid pore-pressure (Shapiro, 2003). The terms of nonlinear elasticity and slow dynamics refer to complex behavior of rocks when submitted to subtle stress–strain changes. These behaviors include nonlinear stress–strain relations, hysteresis and delayed relaxation (Johnson and Rasolofosaon, 1996; Johnson and Jia, 2005). Non-linear damage rheology models have been developed to account for such behaviors (Lyakhovsky et al., 2009).

One of the most convincing in situ observations of rock seismic velocity dependence to stress changes has been obtained underground by Yamamura et al. (2003) who studied seismic velocity dependence to strain induced by oceanic and solid tides in a vault. The authors were able to perform very precise and repetitive measurements of seismic velocity changes induced by tidal compression and dilation using active sources and were able to assess a velocity-stress sensitivity value of 5.10^{-7} Pa^{-1}. The velocity-stress sensitivity also referred as elastic piezosensitivity or seismic velocity susceptibility to transient stress perturbations corresponds to the ratio between relative velocity change and applied stress perturbation ($\frac{\delta v/v}{\delta \sigma}$). The velocity-stress sensitivity is known to be strong at shallow depths (Birch, 1966) and can be significantly increased in rocks characterized by high fluid pore-pressure (low effective pressure, Shapiro, 2003). It can be interpreted as a marker for rock compliance. Monitoring this parameter might be useful for the detection of earthquake nucleation stages (Johnston et al., 2006). Seismic velocity reductions linked to increased pore-pressure induced by the drainage of meteoritic water have also been clearly observed by Hillers et al. (2014). Tsai (2011) proposed a comprehensive model to explain seasonal seismic velocity variations observed by Meier et al. (2010) taking into account thermoelastic stress (Ben-Zion and Leary, 1986), poroelastic stress and loading induced by meteoritic water. On volcanoes we expect that seismic velocities can be affected by changes in stress associated with magma pressurization and transport. Seismic velocities can also be affected by damage of the volcanic edifice associated with volcanic fluid transport and seismicity (Shalev and Lyakhovsky, 2013; Carrier et al., 2015).

4. 4-D probing of volcanoes: the case of Piton de la Fournaise volcano

Piton de la Fournaise (PdF) volcano is a hot spot, shield volcano located on La Réunion island in the Indian ocean (Fig. 2). It erupted
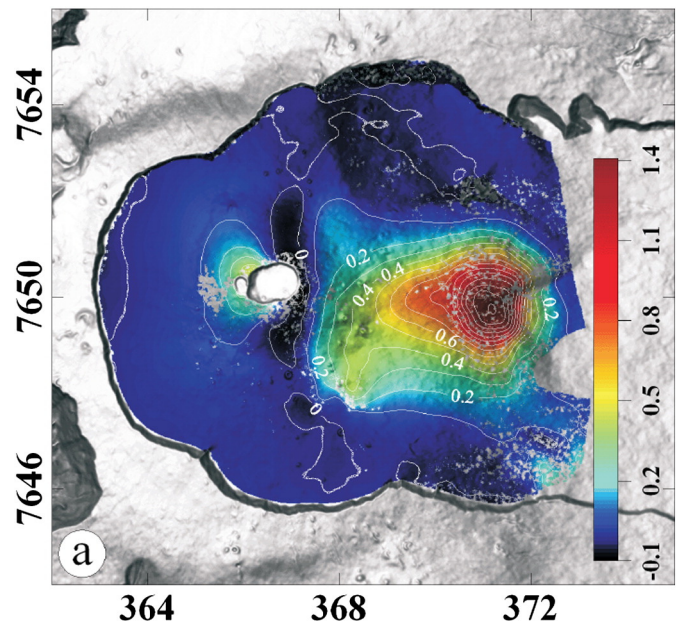
Fig. 6. Eastward horizontal displacement in meters averaged over a period including the April 2007 eruption and crater collapse as observed by InSAR (courtesy of J.L. Froger). Y-axis is Northing ad X-axis is Easting in km.
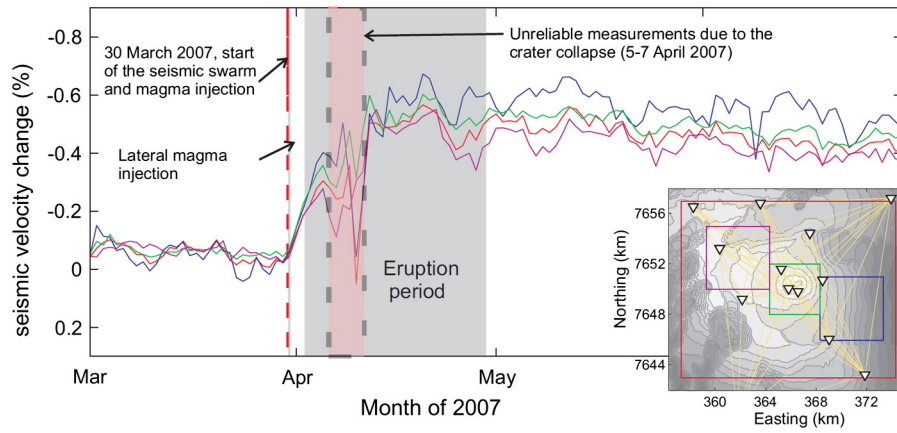
Fig. 7. Seismic velocity changes associated with the April 2007 eruption (Clarke et al., 2013).

more than 30 times between 2000 and 2010. These eruptions lasted from a few hours to a few months and were associated with the emission of mainly basaltic lava with volume ranging from less than one to several tens of million cubic meters (Peltier et al., 2009; Fig. 3). During these last years, 2 major eruptions occurred, namely the March 1998 eruption (60 million cm^3 of lava emitted) and the April 2007 eruption associated with the 300 m high collapse of the main Dolomieu crater and the emission of 130 million cm^3 of lava (Staudacher et al., 2009).

Piton de la Fournaise volcano has been monitored since 1979 by the OVPF/IPGP volcano observatory. In 2009, in the framework of the UnderVolc project (Brenguier et al., 2012), 15 new broad-band seismic stations complemented the observatory seismic network that was composed of about 20 essentially short-period seismic stations. The intense eruptive activity together with a weak tectonic activity makes Piton de la Fournaise volcano a *laboratory* volcano well suited for studies focused on the processes of magma pressurization and injection, and for the development of innovative imaging and monitoring methods.

4.1. The long-term behavior of Piton de la Fournaise volcano inferred from noise-based seismic monitoring

As commonly described in volcanic systems, PdF volcanic activity is driven by long-term aseismic replenishment of magma through the ductile crust and storage at the boundary with the brittle seismogenic crust. The long- to short-term pressure buildup within the storage area preceding eruptions is partly due to this increase of replenished magma volume and also to its crystallization and gas exsolution. Here we will see how seismic noise-based monitoring together with geodetic observations can help to constrain these different long-term mechanisms.

On PdF we have access to continuous seismic data from 2000. Using the methodology described above we measured continuous seismic velocity changes from 2000 to 2013 (Brenguier et al., 2011; Clarke et al., 2013; Rivet et al., 2014). Overall, we observe a long-term velocity decrease preceding the April 2007 eruption, which is followed by a slow velocity increase (Fig. 4). The short-term fluctuations of velocity changes in Fig. 4 are governed by pre-eruptive changes and seasonal variations and will be discussed later.

In Fig. 4, the long-term seismic velocity increase after 2007 corresponds to a long-term contraction of the edifice observed by GPS (Fig. 4, bottom) that can be interpreted as the non-elastic edifice response to the emptying of the magma reservoir at depth during the April 2007 eruption. More interestingly, GPS and seismic velocity change observations differ for the period from 2004 to 2007. Seismic velocity changes show a long-term velocity decrease from 2000 to 2004, which could be related to the long-term pressure buildup of the reservoir due to magma replenishment. This magma replenishment probably

happened continually since the opening of a deep conduit prior to the 1998 eruption (Battaglia et al., 2005). In contrast, seismic velocities do not show any long-term changes from 2004 to 2007, indicating a
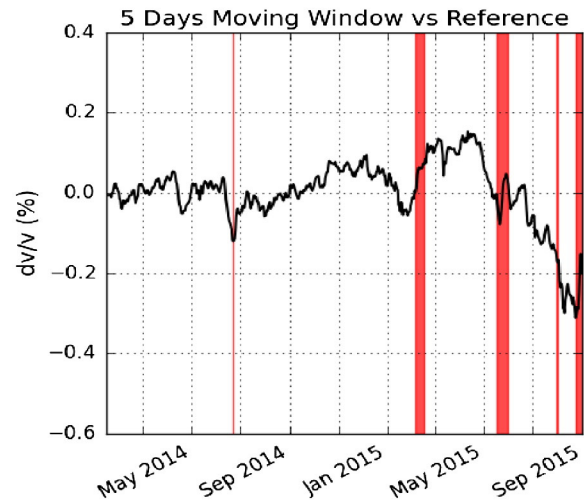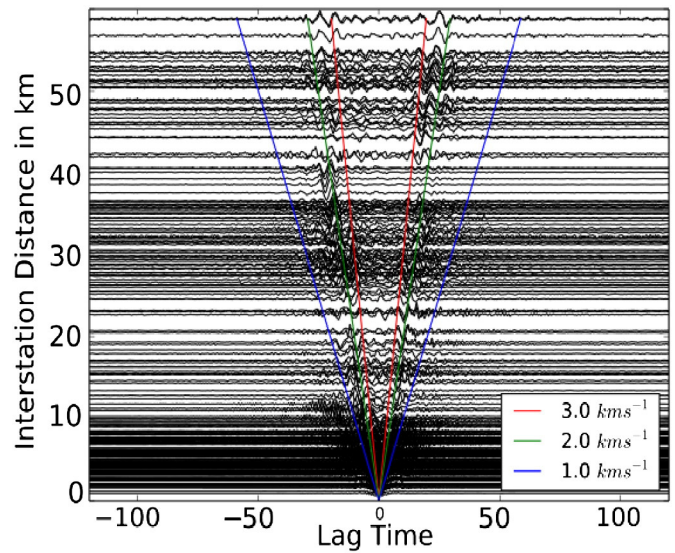
Fig. 8. Examples of outputs from MSNoise. Left, cross-correlations order by interstation distance. Right, seismic velocity changes (%) showing a clear velocity decrease preceding the large August 2015 eruption of PdF. The red bars indicate periods of eruption. (For interpretation of the references to color in this figure legend, the reader is referred to the web version of this article.)
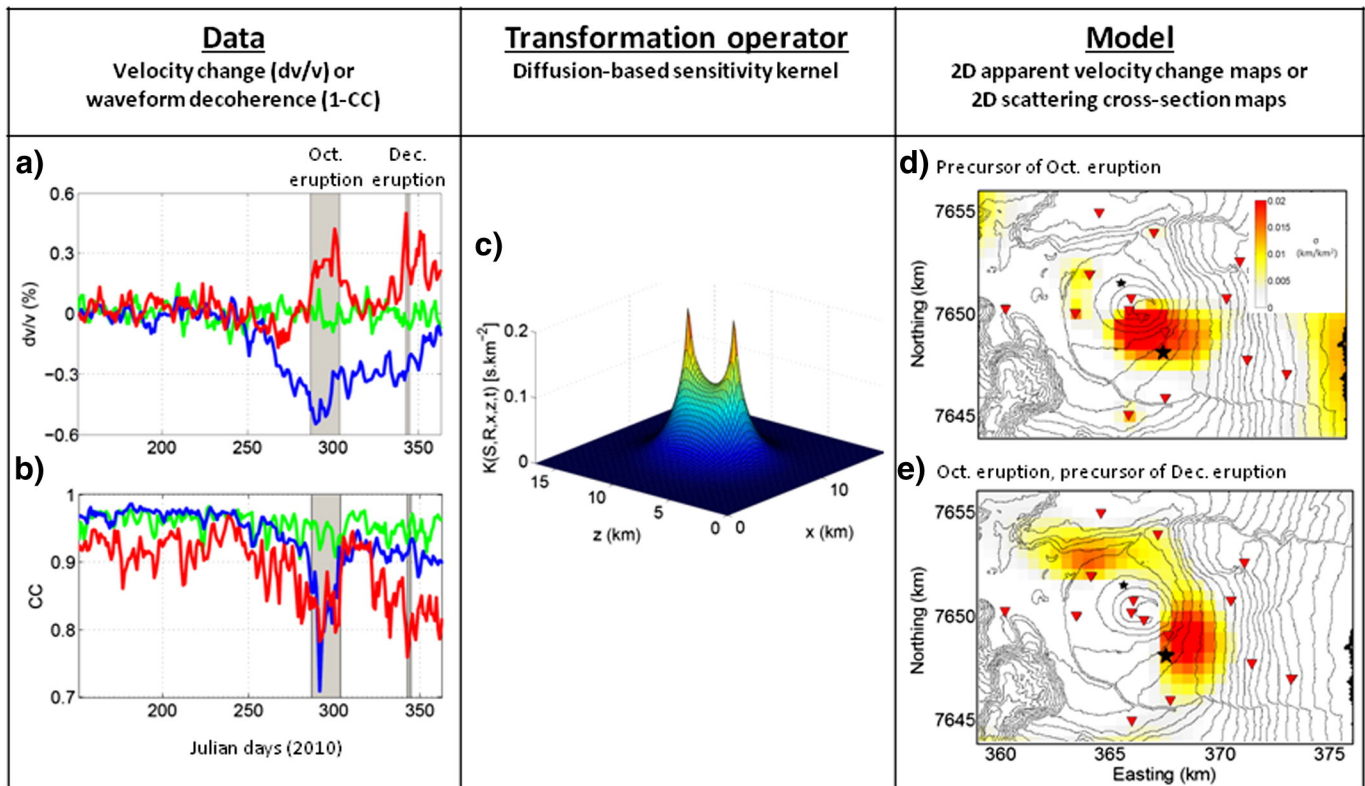
Fig. 9. Schematic view of the imaging procedure. The data in form of velocity changes (a) or waveform decoherence (b) are inverted using diffusion-based sensitivity kernels (c) to obtain 2D maps of the localized changes: (d) showing the localized precursor of the October eruption (big star), (e) showing the October eruption and a precursor of the December eruption (small star). (For interpretation of the references to color in this figure, the reader is referred to the web version of this article.)

possible slowing down of the deep magma transfers and the sealing of the associated magma feeding pathway. Surprisingly, between 2004 and 2007, GPS data show an inter-eruptive edifice inflation (Fig. 4, bottom) whereas seismic velocities are rather constant (we would expect a velocity decrease). Our interpretation is that GPS data are mostly sensitive to near-surface processes whereas seismic velocity changes are sensitive to deeper ones (sensitivity from surface to 3 km depth). The edifice inflation shown by GPS would essentially be due to the effects of shallow magma injections in the pressurized edifice whereas the constancy of seismic velocities would be a marker for the slowing down of the deep magma replenishment following the 1998 eruption.

4.2. The short-term pre-eruptive behavior of Piton de la Fournaise

As observed in Fig. 4, long-term seismic velocity changes are modulated by short-term changes. These are known to be partly due to the loading of meteoritic water that penetrates through the edifice (Sens-Schönfelder and Wegler, 2006). There is however clear indications that short-term velocity decreases occur a few weeks to a few days before eruptions (Brenguier et al., 2008a; Duputel et al., 2009) that have been found to be located in the central, active part of the edifice. They have been interpreted as the rapid pressurization of the edifice prior to eruption (Fig. 5). These transient pre-eruptive velocity reductions are also observed during the post-2007 period characterized by a global velocity increase (Rivet et al., 2015) which proves that these observations are sensitive to different processes at different time scales (e.g. long-term edifice deflation and short-term edifice pressurization, Sens-Schönfelder et al., 2014).

There is still much debate and discussions about the origin of the short-term velocity reductions of the edifice observed here prior to eruptions. In particular, some authors propose relevant processes associated with magma-hydrothermal system interactions that put emphasis on the pressurization of heated and vaporized hydrothermal water

that favor the failure of the magma reservoir cap rock (Lénat et al., 2012; Caudron et al., 2015). In a different direction, Carrier et al. (2015) interpret these velocity decreases as a rapid change of material rheology to non-elastic behavior associated with weakening of the volcanic edifice in pre-eruptive stages.

4.3. Interplay between magmatic activity and the volcanic edifice

In the previous sections we assumed a simple response of the volcanic edifice summit to pressure buildup and emptying of the reservoir in terms of inflation and deflation and related seismic velocity decreases and increases. In this section we will describe how large transient stress perturbations initiated by magma transport at depth may produce large lateral flank deformations and in return how this stress relaxation may drive magma transport at depth. We studied the April 2007 eruption characterized by a very large reduction of seismic velocity (Fig. 4) of almost 1%. As shown in Fig. 6 by InSAR, the East flank of PdF was affected by a large horizontal eastward displacement reaching 1.4 m. However, the precise timing of this movement cannot be derived from InSAR. We thus investigated the short-term seismic velocity changes associated with the April 2007 eruption.

Fig. 7 shows the short-term seismic velocity changes associated with the April 2007 eruption. Overall it shows that the large seismic velocity drop started a few days before the April 2007 eruption, on March 30 when a small eruption lasting a few hours occurred. Together with GPS observations, we showed that the large seismic velocity drop was due to the flank movement and thus that this movement started on March 30 a few days before the April 2 eruption (Clarke et al., 2013). A later numerical study from Got et al. (2013) showed that the stress relaxation by plastic deformation of the East flank could explain such large deformation of the eastern flank and that, in return, this stress relaxation could have favored the horizontal magma migration that led to the distal emission of a large amount of lava during the April 2007
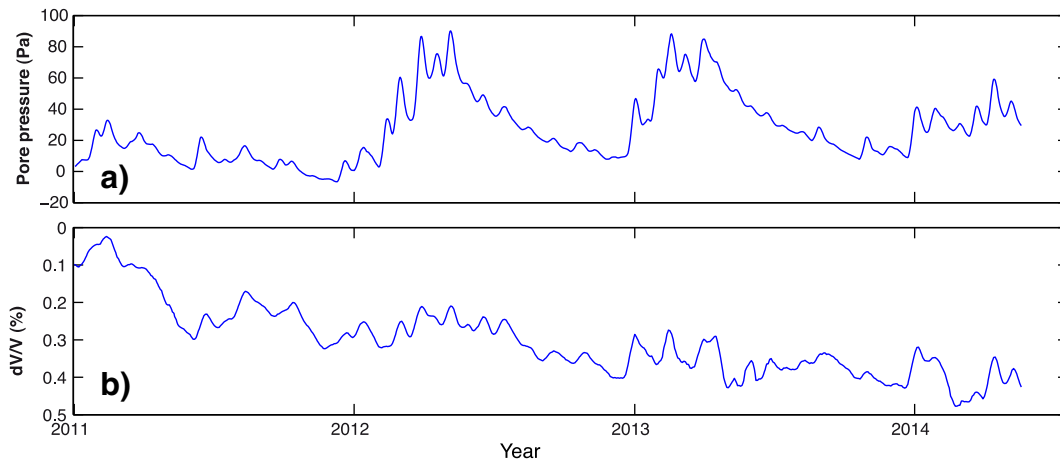
Fig. 10. Comparison between (a) fluid pressure and (b) seismic velocity changes measured on an 8 day moving window during the quiet period with no eruptive activity, between January 2011 and May 2014 (from Rivet et al., 2015).

eruption. The large velocity decrease following the March 30 eruption is thus a marker for anomalous elasto-plastic deformation of the volcanic edifice flank that drove the anomalously large April 2007 distal eruption. In that idea, seismic velocity monitoring from noise can thus be employed to track large volcanic flank movements associated with magma transport close to surface.

4.4. The rise of open source noise-based monitoring: MSNoise

Until recently, the analysis of seismic noise was restricted to laboratory research, far from the real world of real-time monitoring volcanoes. Recently, some huge efforts have been produced to bring research codes and scripts to an operational level. The Piton de la Fournaise has been monitored for seismic velocity changes since 2010 using a set of shell, Matlab and C codes, which have been replaced by MSNoise (http://www.msnoise.org/, Lecocq et al., 2014) in June 2014. The MSNoise package has been designed to work automatically on existing seismic data, independently of its structure or format. This can only be done thanks to the rise of Open Source software and libraries, like ObsPy (Krischer et al., 2015), scipy, matplotlib and numpy running in Python. Fast and efficient codes can be written in Python, so for most usages, it is not necessary to run slightly more efficient FORTRAN or C codes. On a daily basis, MSNoise scans the data archive for new or modified content, computes cross-correlations and compares each daily stack to a pre-defined reference to obtain relative velocity variations (dv/v). Currently, MSNoise only computes dv/v, but industry/university funded efforts are being made to add the mapping and inversion of the velocity and the dv/v in the same automatic fashion.

Since 2014, MSNoise monitors automatically the dv/v under the Piton de la Fournaise using only ZZ cross-correlations between broadband seismometers. The part of the cross-correlation function used to compute the dv/v starts at the theoretical arrival time of a wave traveling at 1 km/s between the two stations, e.g. 2 s for stations located 2 km apart. This avoids including ballistic arrivals and greatly reduces the observed seasonal effects (see Fig. 8).

Five eruptions occurred since the installation of MSNoise at the PdF. They were all preceded by seismic velocity decreases but in some case (Feb. 2015), these velocity drops could also be related to the rainfall effect (Rivet et al., 2015). It will be an important task in the future to implement the correction of the rainfall effect in real time.

4.5. Conclusions

In conclusion, we were able to assess from noise-based monitoring that the PdF volcano shallow magma reservoir was probably fed continuously from the 1998 eruption to about 2004 and that the conduit

opened in 1998 then sealed in 2004. We were also able to observe the short-term phases of rapid pressure buildup within the reservoir before eruptions and showed that, above a level of stress increase, plastic deformation would take place on the eastern flank and that the associated stress release would favor the migration of magma laterally and the emission of a large volume of magma. Even though these observations are quite unique, some other groups have obtained similar observations of noise-based seismic velocity changes during unrest volcanic periods in other volcanic contexts (Baptie, 2010; Bennington et al., 2015).

5. Perspectives for improving high-resolution 4-D probing of volcanoes

Throughout this manuscript, we showed observations of velocity changes averaged at depth over the first few kilometers of the subsurface. Our observations thus correspond to an averaged contribution of different processes occurring at different depths with different intensities. For example on volcanoes, our observations are a combination of effects of water content due to rainfall in the near subsurface, short-term magma pressure buildup and transport in the edifice and long-term deep magma replenishment and pressure buildup. In active tectonic domains, we showed that, in particular, our observations were composed of effects of shaking due to seismic waves and effects of deep stress perturbations due to for example viscoelastic deformation. Deciphering these different processes is of primary importance for improving our ability to forecast eruptive behavior at a long-term or to characterize viscoelastic flow in the lower crust and related rheology. One of the key points of our method would be to better understand the sensitivity of our measurements laterally and at depth. In the following we discuss future directions for improving the detection of magmatic processes at depth using seismic noise correlations.

5.1. Localization of medium changes within the volcano edifice using the diffuse character of coda waves

Forecasting the location of an eruption is of primary importance for risk management in volcanic regions. Locating the underground structural changes associated with a potential eruption is also a key issue to better understand the dynamics at work in a volcano. The installation of the additional stations from the UnderVolc network in 2009 (Brenguier et al., 2012) made possible the application of a recently developed imaging procedure (Larose et al., 2010; Planès et al., 2014, 2015) based on the sensitivity of multiply scattered waves to weak changes in the medium.

We hence studied the 2010 October (lasting for 2 weeks) and December (lasting for 2 days) eruptions of Piton de La Fournaise that
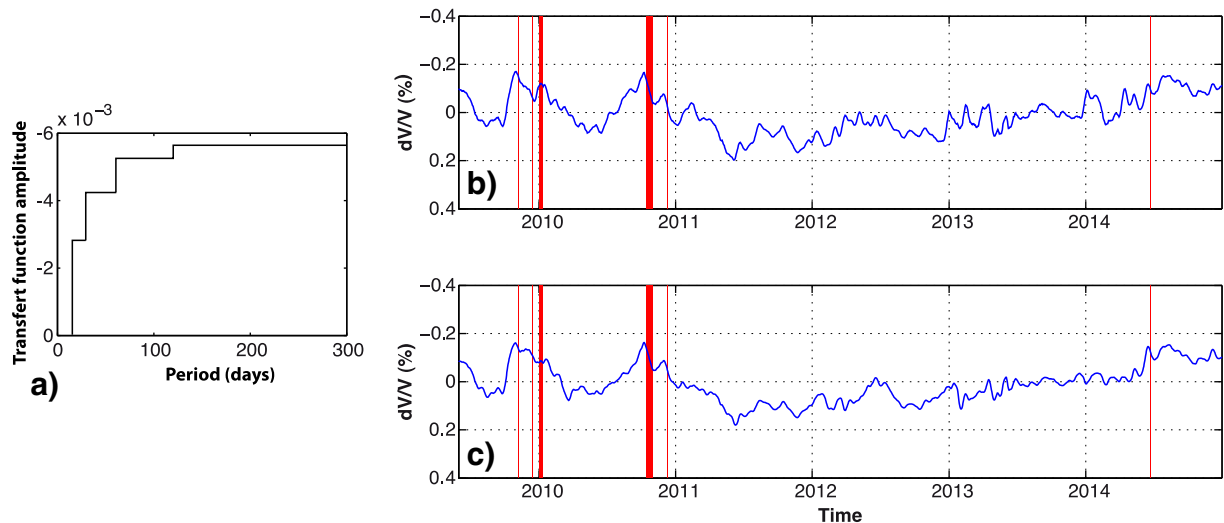
Fig. 11. (a) Transfer function between fluid pressure and seismic velocity changes estimated from the 2011–2012 time series. Seismic velocity changes measured at PdF volcano (b) without and (c) with a correction of rainfall effects. Note that on both time series the long-term trend of increasing velocity has been removed. The vertical red bars mark the periods of eruptive activity (from Rivet et al., 2015). (For interpretation of the references to color in this figure legend, the reader is referred to the web version of this article.)

occurred on opposite sides of the volcanic edifice (black stars in Fig. 9d, e, Obermann et al., 2013b) with the goal of locating the eruptions and possible precursors. We calculated the noise cross correlations between the available 19 broadband sensors (red triangles in Fig. 9d, e) and studied two types of changes in the coda: apparent velocity variations related to changes in the elastic properties of the medium (Fig. 9a); and, waveform decoherence associated with variations in the scattering, and thus the geological structures (Fig. 9b). We observed that the temporal variations of both of these parameters provided potential precursors of volcanic eruptions at Piton de la Fournaise (Fig. 9a, b, Obermann et al. (2013b)). The evolution of the velocity changes and the waveform coherence for the 3 exemplary station couples depicted in Fig. 9a, b; pairs indicated in Fig. 9d; shows a clear spatial dependency that we use for the location of the medium changes.

Contrary to the propagation of direct waves that can be described with classical wave equations, coda wave propagation resembles a random walk process. Under the assumption that the coda is dominated by surface waves, the propagation can be approximated with the 2D solution of the diffusion equation. We hence created sensitivity kernels (Fig. 9c, Pacheco and Snieder, 2005) between all the station pairs that relate the observed changes to a local medium perturbation in the volcanic edifice. We use a linear least-squares inversion scheme (Tarantola and Valette, 1982) to obtain the horizontal distribution of the changes (Fig. 9d, e, Obermann et al., 2013b).

The localizations from the preeruptive and coeruptive changes are in good agreement with the actual eruptive activities (Fig. 9d, e). However, as we assumed that the early coda of the correlations is dominated by surface waves, a 2D sensitivity kernel was used to describe the diffusive wave propagation and the localization is hence limited to the horizontal plane. Obermann et al. (2013a) have shown that there is a significant contribution of body waves (3D propagation) in strongly heterogeneous media, such as volcanoes. Ongoing studies to implement body and surface wave propagation in a 3D sensitivity kernel might yield the possibility in the future to also locate changes in the volcanic edifice at depth and to possibly improve resolution (Obermann et al., 2016).

5.2. Rainfall effect correction for improved precursory velocity change detection

Environmental effects such as rainfall can trigger and modulate a series of geological phenomenon through hydromechanical coupling. For instance fluid pressure diffusion subsequent to rainfall episodes has

been proposed to be responsible for induced seismicity (e.g. Muco, 1995; Hainzl et al., 2006, 2013; Kraft et al., 2006; Svejdar et al., 2011). Similarly pore pressure change at depth due to atmospheric perturbations can affect seismic wave velocities (Sens-Schönfelder and Wegler, 2006; Meier et al., 2010; Tsai, 2011; Froment et al., 2013; Hillers et al., 2014; Gassenmeier et al., 2015; Rivet et al., 2015). A critical point is that the same way as magma pressurization produces seismic velocity changes, pore pressure changes can lead to seismic velocity change with similar duration and amplitude as the eruptive precursory signals (Rivet et al., 2015). Therefore it is essential to minimize seismic velocity changes related to environmental effects to increase the detection of seismic velocity changes caused by precursory magmatic movement before volcanic eruptions.

Between 2011 and 2014, during a quiet period of the PdF volcano characterized by a lower volcanic activity (Roult et al., 2012) we investigated the origin of the seismic wave velocity variations. We estimated pore pressure change produced by rainfall considering only the direct effect of diffusion following similar approaches previously used to study the potential links between rainfall and seismicity (Hainzl et al., 2006; Kraft et al., 2006; Talwani et al., 2007) as well as seismic velocity changes (Sens-Schönfelder and Wegler, 2006; Hillers et al., 2014). Fig. 10 presents the averaged fluid pressure change estimated between 0 and 6 km depth and the seismic velocity changes over the same period. Short-term velocity decreases (i.e., 1–2 months long) are well correlated with increases in fluid pressure due to rainfall episodes. We further explored the relationship between fluid pressure change and seismic velocity changes; in particular we determined which period bands of the seismic velocity variations are affected by changes in fluid pressure. For a two year period with no eruption, high correlation coefficients of 0.84 and 0.73 were found between seismic velocity and pore pressure changes for the bands 60–30 and 30–16 days suggesting that velocity changes were mainly due to fluid pressure changes.

We then modeled seismic velocity changes induced by fluid pressure changes using a signal-processing approach. Because the mechanics by which a fluid pressure changes produce a seismic velocity variations are not well constrained, we choose to build a transfer function between both variables during a period with no volcanic activity (Fig. 11a). The transfer function is the description of the input–output relation for a linear system, in our case between the fluid pressure change and the seismic velocity change, respectively. For each period band for which we observe a correlation, we assume that seismic velocity change is proportional to fluid pressure. We applied the transfer
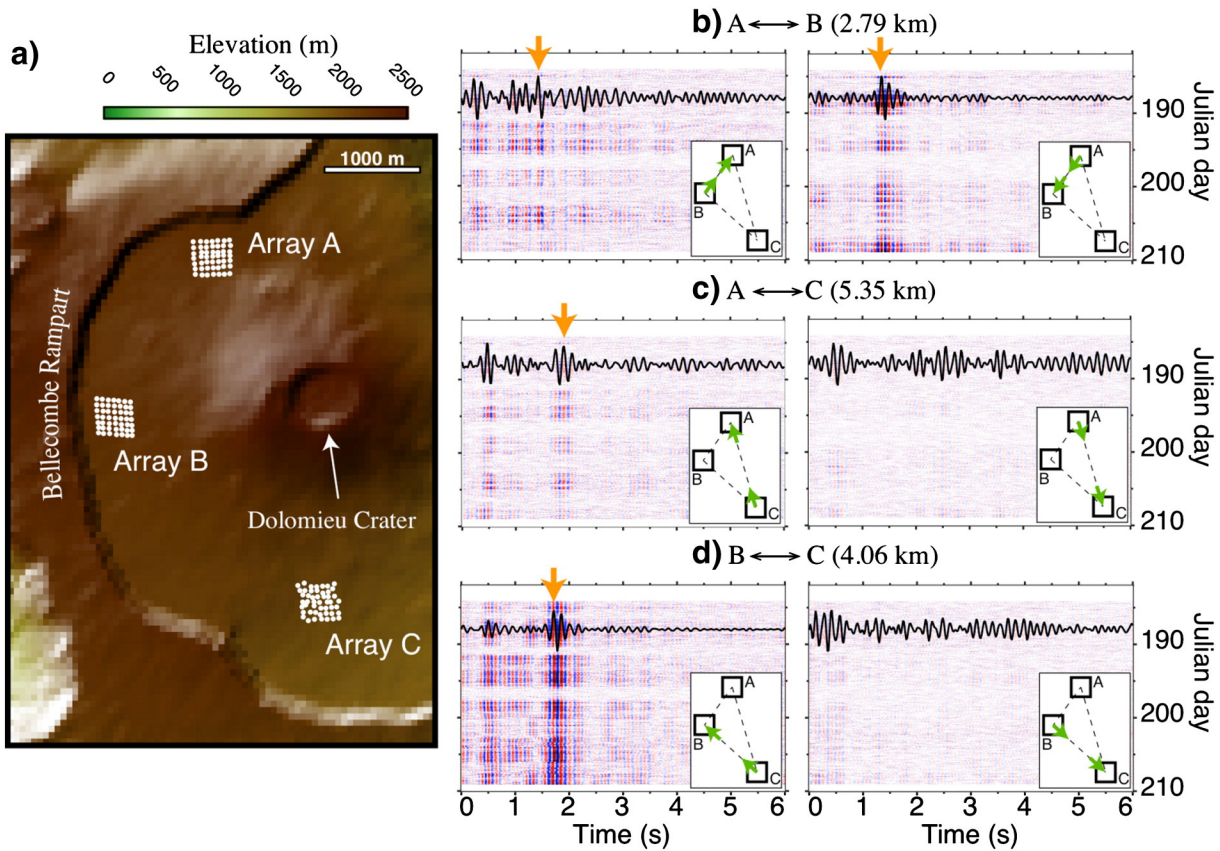
Fig. 12. a) Map of the 3 arrays deployed during the VolcArray experiment. White dots correspond to geophones. Each array has 7-by-7 receivers. b to d) Hourly traces between 6 and 12 Hz after applying DBF processing in the azimuth of direct paths between source and receiver arrays (green arrows inside corresponding inset). Each panel corresponds to a one-way propagation between 2 arrays. Black traces are the stacked waveforms over all hourly traces. Orange arrows show direct body waves (modified from Nakata et al., 2016). (For interpretation of the references to color in this figure legend, the reader is referred to the web version of this article.)

function to the fluid pressure and obtain a synthetic seismic velocity change time series that accounts for the fluid pressure change effects during rainfall.

Finally, we corrected a 5.5 years seismic velocity change time series from fluid pressure change effects by subtracting the synthetic seismic velocity changes produced by rainfall. Fig. 11b, c presents the detrended seismic velocity change time series before and after the correction of rainfall effect was applied. While seismic velocity changes associated with eruptions are conserved, during the quiet period, the amplitude of fluctuations reduces by about 20%. The residual fluctuations can arise from an incomplete correction of meteorological effects or can be some random fluctuations and/or undetected velocity changes associated with deeper phenomena. Finally we found a pre-eruptive seismic velocity drop (0.15%) undetected before correction associated with the 21 June 2014 eruption. Indeed several large seismic velocity decreases produced by large rainfall episodes in 2014 were reduced. The correction of rainfall effects makes it possible to detect seismic velocity change precursory signals that were hidden because of environmental fluctuations of the seismic velocity.

5.3. Body-wave extraction using dense arrays

Another complementary approach to infer direct information about ongoing magmatic process at depth is to extract body-waves from noise correlations. Compared to body-wave tomography and considering similar wavelengths, surface wave tomography succeeds in retrieving lateral sub-surface velocity contrasts but is less efficient in resolving velocity perturbations at depth. The use of Large-N seismic arrays has proven to be of great benefit for extracting noisy body-waves from noise-correlations by stacking over a large number of receiver pairs

and by applying array processing. Different studies show that such noise-based body-wave extraction is possible at various scales (Draganov et al., 2009; Poli et al., 2012). Recently, Nakata et al. (2015) were able to implement the first 3-D P-wave velocity tomography from continuous ground motion recorded on a dense array of more than 2500 seismic sensors installed at Long Beach (California, USA). Added to a more traditional surface wave approach, such applications significantly improve our knowledge of the subsurface by obtaining a constraint on the bulk modulus and by improving the spatial resolution.

Following this idea, we conducted a Large-N array experiment on the Piton de la Fournaise volcano. During this so-called VolcArray experiment, about 300 vertical-component geophones were deployed at 152 locations and continuously observed ground motion for 30 days (Brenguier et al., 2016). Three dense arrays (A, B, and C), each made by 7 × 7 receivers, were installed about 1.5 km away from the Dolomieu crater on the North, West and South side, respectively (Fig. 12a). The main goal of this experiment was to extract body waves from the ambient noise cross-correlations, traveling through the vicinity of the active magma reservoir located about 2.5 km deep beneath the main crater (Peltier et al., 2009).

Because heterogeneities are strong below the main crater, we expect such body waves to be difficult to extract and interpret due to, for example, scattering and multi-pathing effects compared to other areas of ambient-noise studies. The VolcArray experiment was designed in such a way that array-processing techniques can be performed to enhance the signal-to-noise ratio (SNR) and help our understanding of the wavefields. Being able to separate body waves from surface waves, or to identify different wave paths within the medium will be extremely useful to increase the spatial resolution of both imaging and monitoring applications. Using array processing to improve SNR can also lead to a
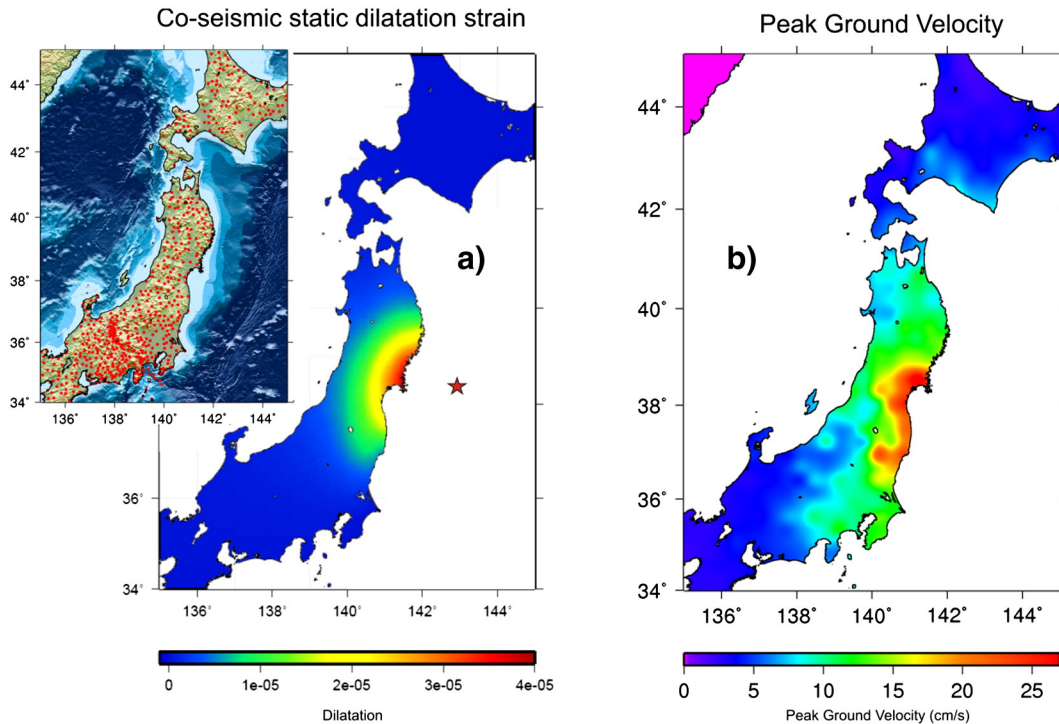
Fig. 13. A) Modeled co-seismic dilatation static strain at 5 km depth. The red star shows the position of the Tohoku-oki earthquake epicenter. Inset figure shows the position of the used Hi-net seismic stations (red points). B) Averaged Peak Ground Velocity measured using the KiK-net strong-motion network (from Brenguier et al., 2014). (For interpretation of the references to color in this figure legend, the reader is referred to the web version of this article.)

better temporal resolution for monitoring applications since we can reduce the amount of time to obtain stable waveforms to estimate time-lapse velocity changes.

Among all possible array-processing techniques, here we choose Double Beamforming (DBF) to efficiently use the multiple array configurations (Rost and Thomas, 2002; Boué et al., 2013), and hence each array is turned either as a source or a receiver array. Following a simple slant-stack approach, DBF can be considered as a spatial filter that decomposes the wavefield as a function of both the takeoff (source side) and incident (receiver side) ray-parameters. With 2D arrays, the (apparent) ray-parameter is defined by its azimuth and velocity (or slowness). By applying DBF, instead of using station-to-station correlations, we rather use array-to-array beams to look for body waves that propagate in specific directions (Eigen-rays).

Fig. 12b, c, d shows DBF cross-correlation (6-12 Hz) between the 3 combinations of array (A to B, A to C and B to C) and for the 2 directions of propagation. In this example, we fixed the azimuth to the direction of the green arrows in the figure in order to focus on the ballistic path between arrays. These figures show that we successfully extract fast body waves between the 3 combinations of arrays including the wave that propagates beneath the main crater of the volcano (from C to A). Propagations from A to C and from B to C do not show clear body waves due to a lack of coherence of the initial ambient noise wave field in these directions. The very fast arrival waves (e.g., 0.5 s waves in Fig. 12c) are caused by uneven source distributions (Nakata et al., 2016). Also this DBF processing is applied on hourly cross-correlations, and we extract coherent body waves in each hour, which means that we can use these body waves for high resolution monitoring applications by measuring their travel time perturbations day after day.

6. The susceptibility of volcanoes to shaking from seismic waves

The rise of 4-D noise-based seismology has led to an interesting new observation that is the level of seismic velocity decrease induced by

shaking associated with passing seismic waves. This observation, called seismic susceptibility, has been widely mapped for the first time in Japan and has been shown to be anomalous in volcanic regions. We describe herewith some details of this study.

The Tohoku-oki earthquake is the best ever recorded giant earthquake worldwide. It was associated with large widespread static ground deformation and ground shaking (Fig. 13). We used seismic noise-based monitoring to characterize the response of the upper crust to co-seismic shaking and deformation caused by the Tohoku-oki earthquake. We analyzed one year of continuous seismic records from a portion of the dense Hi-net seismic network (600 stations shown in Fig. 13A) spanning 6 months before and 6 months after the earthquake occurrence.

Fig. 14A shows the coseismic velocity reductions over Honshu, Japan. The most striking feature of this figure is that the strongest velocity drops are not observed in the area closest to the epicenter or within large sedimentary basins, as one could expect. The patterns of observed velocity reductions do not correlate with the intensity of ground shaking or with co-seismic deformation (Fig. 13). The strongest co-seismic velocity reductions occur under volcanic regions. In particular, a large part of the Tohoku volcanic front and the Mt. Fuji volcanic region are well delineated. We then compute what we call seismic velocity susceptibility as the locally measured coseismic crustal velocity reductions normalized by the local dynamic stress perturbations estimated using PGV observations (Brenguier et al., 2014). Fig. 14B shows low susceptibility values in regions of stiff, old plutonic rocks (a few 10^{-4} MPa^{-1}) but in contrast shows high seismic velocity susceptibility values in volcanic regions (10^{-3} MPa^{-1}).

Under volcanic areas, the effective pressure in the crust can be reduced because of the presence of highly pressurized hydrothermal and magmatic volcanic fluids at depth. The sensitivity of seismic velocities to stress changes in rocks increases with decreasing effective pressure (Zinszner et al., 1997; Shapiro, 2003). We thus argue that the observed strong co-seismic velocity reductions delineate the regions where such pressurized volcanic fluids are present in the upper crust. An important implication of our observation is that the seismic velocity
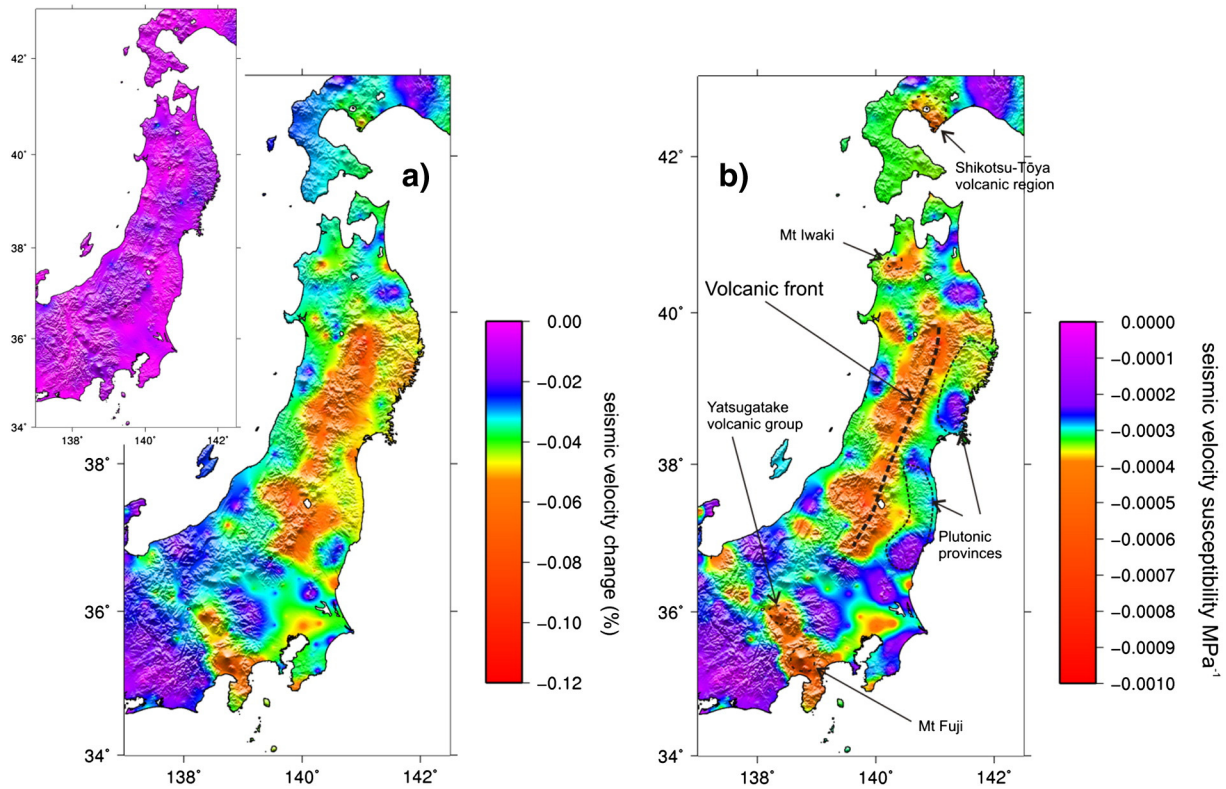
Fig. 14. A) Co-seismic crustal seismic velocity changes induced by the 2011 Tohoku-oki earthquake. The inset figure shows velocity changes averaged over 4 days preceding the Tohoku-oki earthquake. B) Seismic velocity susceptibility computed using seismic velocity changes shown in A (Brenguier et al., 2014).

susceptibility to stress perturbations can be used as a proxy to the level of pressurization of hydrothermal and/or magmatic fluids in volcanic areas. So far, this susceptibility is maximized in the Mt. Fuji area and along the Tohoku volcanic arc where it reaches 15×10^{-4} MPa^{-1} whereas it is ten times smaller for the stiff Cretaceous plutonic regions of the Eastern Tohoku (Fig. 14B).

Previous works also reported seismic velocity drop observations associated with seismic shaking at volcanoes (Battaglia et al., 2012; Lesage et al., 2014). This result in Japan is however, to the best of our knowledge, the first observation of high seismic velocity susceptibility under volcanoes. Chaves and Schwartz (2016) report a second observation of this kind in the seismogenic part of the subduction zone below Costa Rica highlighting the interest of this new approach to detect and characterize regions of high fluid pore pressure in the crust.

7. Conclusions

4D noise-based seismology at volcanoes is thus highly promising as for example detecting early markers of volcanic unrest. However, this method still suffers from a lack of adequate vertical resolution that would be required in order to discriminate between processes occurring near surface such as rainfall perturbations or deeper such as magma pressure buildup. The rise of dense seismic arrays and unaliased seismic wavefield experiments such as recently the iMUSH or the Socorro Magma Body seismic projects will certainly contribute to partially resolve this issue. By improving the passive reconstruction of direct or reflected body-waves propagating in the vicinity of magma reservoirs using arrays of arrays we hope to improve our understanding of the complex processes of volcanic eruption triggering. These developments will serve the broader field of monitoring fluid transport and pressure buildup at depth and for example the related applications of geothermal resource production or industrial waste-water injection.

References

Aki, K., 1957. Space and time spectra of stationary stochastic waves, with special reference to microtremors.

Baig, A.M., Campillo, M., Brenguier, F., 2009. Denoising seismic noise cross correlations. J. Geophys. Res. Solid Earth 114 (B8) (1978–2012).

Ballmer, S., Wolfe, C.J., Okubo, P.G., Haney, M.M., Thurber, C.H., 2013. Ambient seismic noise interferometry in Hawai'i reveals long-range observability of volcanic tremor. Geophys. J. Int. 194, 512–523.

Baptie, B.J., 2010. Lava dome collapse detected using passive seismic interferometry. Geophys. Res. Lett. 37 (19).

Battaglia, J., Ferrazzini, V., Staudacher, T., Aki, K., Cheminée, J.L., 2005. Pre-eruptive migration of earthquakes at the Piton de la Fournaise volcano (Réunion Island). Geophys. J. Int. 161 (2), 549–558.

Battaglia, J., Métaxian, J.P., Garaebiti, E., 2012. Earthquake-volcano interaction imaged by coda wave interferometry. Geophys. Res. Lett. 39 (11).

Bennington, N.L., Haney, M., De Angelis, S., Thurber, C.H., Freymueller, J., 2015. Monitoring changes in seismic velocity related to an ongoing rapid inflation event at Okmok volcano, Alaska. J. Geophys. Res. Solid Earth 120 (8), 5664–5676.

Ben-Zion, Y., Leary, P., 1986. Thermoelastic strain in a half-space covered by unconsolidated material. Bull. Seismol. Soc. Am. 76 (5), 1447–1460.

Birch, F., 1966. Section 7: compressibility; elastic constants (see also section 9). Geol. Soc. Am. Mem. 97, 97–174.

Boué, P., Roux, P., Campillo, M., de Cacqueray, B., 2013. Double beamforming processing in a seismic prospecting context. Geophysics 78 (3), V101–V108.

Brenguier, F., Shapiro, N.M., Campillo, M., Nercessian, A., Ferrazzini, V., 2007. 3-D surface wave tomography of the Piton de la Fournaise volcano using seismic noise correlations. Geophys. Res. Lett. 34 (2).

Brenguier, F., Shapiro, N.M., Campillo, M., Ferrazzini, V., Duputel, Z., Coutant, O., Nercessian, A., 2008a. Towards forecasting volcanic eruptions using seismic noise. Nat. Geosci. 1 (2), 126–130.

Brenguier, F., Campillo, M., Hadziioannou, C., Shapiro, N.M., Nadeau, R.M., Larose, E., 2008b. Postseismic relaxation along the San Andreas fault at Parkfield from continuous seismological observations. Science 321 (5895), 1478–1481.

Brenguier, F., Clarke, D., Aoki, Y., Shapiro, N.M., Campillo, M., Ferrazzini, V., 2011. Monitoring volcanoes using seismic noise correlations, 2011. Compt. Rendus Geosci. 343 (2011), 633–638.

Brenguier, F., Kowalski, P., Staudacher, T., Ferrazzini, V., Lauret, F., Boissier, P., ... Di Muro, A., 2012. First results from the UnderVolc high resolution seismic and GPS network deployed on Piton de la Fournaise volcano. Seismol. Res. Lett. 83 (1), 97–102.

Brenguier, F., Campillo, M., Takeda, T., Aoki, Y., Shapiro, N.M., Briand, X., ... Miyake, H., 2014. Mapping pressurized volcanic fluids from induced crustal seismic velocity drops. Science 345 (6192), 80–82.

Brenguier, F., Kowalski, P., Ackerley, N., Nakata, N., Boué, P., Campillo, M., ... Roux, P., 2016. Toward 4D noise-based seismic probing of volcanoes: perspectives from a large-N experiment on Piton de la Fournaise volcano. Seismol. Res. Lett. 87 (1), 15–25.

Campillo, M., Paul, A., 2003. Long-range correlations in the diffuse seismic coda. Science 299 (5606), 547–549.

Campillo, M., 2006. Phase and correlation in random seismic fields and the reconstruction of the green function. Pure Appl. Geophys. 163 (2–3), 475–502.

Caricchi, L., Annen, C., Blundy, J., Simpson, G., Pinel, V., 2014. Frequency and magnitude of volcanic eruptions controlled by magma injection and buoyancy. Nat. Geosci. 7 (2), 126–130.

Carrier, A., Got, J.L., Peltier, A., Ferrazzini, V., Staudacher, T., Kowalski, P., Boissier, P., 2015. A damage model for volcanic edifices: implications for edifice strength, magma pressure, and eruptive processes. J. Geophys. Res. Solid Earth 120 (1), 567–583.

Caudron, C., Lecocq, T., Syahbana, D.K., McCausland, W., Watlet, A., Camelbeeck, T., Bernard, A., 2015. Stress and mass changes at a "wet" volcano: example during the 2011–2012 volcanic unrest at Kawah Ijen volcano (Indonesia). J. Geophys. Res. Solid Earth 120 (7), 5117–5134.

Cayol, V., Dieterich, J.H., Okamura, A.T., Miklius, A., 2000. High magma storage rates before the 1983 eruption of Kilauea, Hawaii. Science 288 (5475), 2343–2346.

Chang, W.L., Smith, R.B., Wicks, C., Farrell, J.M., Puskas, C.M., 2007. Accelerated uplift and magmatic intrusion of the Yellowstone caldera, 2004 to 2006. Science 318 (5852), 952–956.

Chaves, E.J., Schwartz, S.Y., 2016. Monitoring transient changes within overpressured regions of subduction zones using ambient seismic noise. Sci. Adv. 2 (1), e1501289.

Clarke, D., Zaccarelli, L., Shapiro, N.M., Brenguier, F., 2011. Assessment of resolution and accuracy of the Moving Window Cross Spectral technique for monitoring crustal temporal variations using ambient seismic noise. Geophys. J. Int. 186 (2), 867–882.

Clarke, D., Brenguier, F., Froger, J.L., Shapiro, N.M., Peltier, A., Staudacher, T., 2013. Timing of a large volcanic flank movement at Piton de la Fournaise volcano using noise-based seismic monitoring and ground deformation measurements. Geophys. J. Int. 195 (2), 1132–1140.

Colombi, A., Chaput, J., Brenguier, F., Hillers, G., Roux, P., Campillo, M., 2014. On the temporal stability of the coda of ambient noise correlations. Compt. Rendus Geosci. 346 (11), 307–316.

Draganov, D., Campman, X., Thorbecke, J., Verdel, A., Wapenaar, K., 2009. Reflection images from ambient seismic noise. Geophysics 74 (5), A63–A67.

Droznin, Shapiro, N.M., Droznina, S.Y., Senyukov, S.L., Chebrov, V.N., Gordeev, E.I., 2015. Detecting and locating volcanic tremors on the Klyuchevskoy group of volcanoes (Kamchatka) based on correlations of continuous seismic records. Geophys. J. Int. 203, 1001–1010. http://dx.doi.org/10.1093/gji/ggv342.

Duputel, Z., Ferrazzini, V., Brenguier, F., et al., 2009. Real time monitoring of relative velocity changes using ambient seismic noise at the Piton de la Fournaise volcano (La Reunion) from January 2006 to June 2007. J. Volcanol. Geotherm. Res. 184 (1–2), 164–173 Special Issue Pages:.

Egle, D.M., Bray, D.E., 1976. Measurement of acoustoelastic and third-order elastic constants for rail steel. J. Acoust. Soc. Am. 60 (3), 741–744.

Froment, B., Campillo, M., Chen, J.H., Liu, Q.Y., 2013. Deformation at depth associated with the 12 May 2008 Mw 7.9 Wenchuan earthquake from seismic ambient noise monitoring. Geophys. Res. Lett. 40, 78–82. http://dx.doi.org/10.1029/2012GL053995.

Gassenmeier, M., Sens-Schönfelder, C., Delatre, M., Korn, M., 2015. Monitoring of environmental influences on seismic velocity at the geological storage site for CO2 in Ketzin (Germany) with ambient seismic noise. Geophys. J. Int. 200 (1), 524–533.

Gerst, A., Savage, M.K., 2004. Seismic anisotropy beneath Ruapehu volcano: a possible eruption forecasting tool. Science 306 (5701), 1543–1547.

Got, J.L., Peltier, A., Staudacher, T., Kowalski, P., Boissier, P., 2013. Edifice strength and magma transfer modulation at Piton de la Fournaise volcano. J. Geophys. Res. Solid Earth 118 (9), 5040–5057.

Grêt, A., Snieder, R., Aster, R.C., Kyle, P.R., 2005. Monitoring rapid temporal change in a volcano with coda wave interferometry. Geophys. Res. Lett. 32 (6).

Hainzl, S., Kraft, T., Wassermann, J., Igel, H., 2006. Evidence for rain-triggered earthquake activity. Geophys. Res. Lett. 33, L19303. http://dx.doi.org/10.1029/2006GL027642.

Hainzl, S., Zakharova, O., Marsan, D., 2013. Impact of aseismic transients on the estimation of aftershock productivity parameters. Bull. Seismol. Soc. Am. 103 (3), 1723–1732. http://dx.doi.org/10.1785/0120120247.

Hadziioannou, C., Larose, E., Coutant, O., Roux, P., Campillo, M., 2009. Stability of monitoring weak changes in multiply scattering media with ambient noise correlation: laboratory experiments. J. Acoust. Soc. Am. 125 (6), 3688–3695.

Hillers, G., Ben-Zion, Y., 2011. Seasonal variations of observed noise amplitudes at 2–18 Hz in southern California. Geophys. J. Int. 184 (2), 860–868.

Hillers, G., Campillo, M., Ma, K.F., 2014. Seismic velocity variations at TCDP are controlled by MJO driven precipitation pattern and high fluid discharge properties. Earth Planet. Sci. Lett. 391, 121–127.

Hughes, D.S., Kelly, J.L., 1953. Second-order elastic deformation of solids. Phys. Rev. 92, 1145–1149.

Husen, S., Smith, R.B., Waite, G.P., 2004. Evidence for gas and magmatic sources beneath the Yellowstone volcanic field from seismic tomographic imaging. J. Volcanol. Geotherm. Res. 131 (3), 397–410.

Ikuta, R., Yamaoka, K., Miyakawa, K., Kunitomo, T., Kumazawa, M., 2002. Continuous monitoring of propagation velocity of seismic wave using ACROSS. Geophys. Res. Lett. 29 (13) 5-1.

Jaxybulatov, K., Shapiro, N.M., Koulakov, I., Mordret, A., Landès, M., Sens-Schönfelder, C., 2014. A large magmatic sill complex beneath the Toba caldera. Science 346 (6209), 617–619.

Johnson, P.A., Rasolofosaon, P.N.J., 1996. Nonlinear elasticity and stress-induced anisotropy in rock. J. Geophys. Res. Solid Earth 101 (B1), 3113–3124 (1978–2012).

Johnson, P.A., Jia, X., 2005. Nonlinear dynamics, granular media and dynamic earthquake triggering. Nature 437 (7060), 871–874.

Johnston, M.J.S., Borcherdt, R.D., Linde, A.T., Gladwin, M.T., 2006. Continuous borehole strain and pore pressure in the near field of the 28 September 2004 M 6.0 Parkfield, California, earthquake: implications for nucleation, fault response, earthquake prediction, and tremor. Bull. Seismol. Soc. Am. 96 (4B), S56–S72.

Kedar, S., Webb, F.H., 2005. The ocean's seismic hum. Science 307 (5710), 682–683.

Koulakov, I., 2013. Studying deep sources of volcanism using multiscale seismic tomography. J. Volcanol. Geotherm. Res. 257, 205–226.

Kraft, T., Wassermann, J., Igel, H., 2006. High-precision relocation and focal mechanism of the 2002 rain-triggered earthquake swarms at Mt. Hochstaufen, SE Germany. Geophys. J. Int. 167, 1513–1528. http://dx.doi.org/10.1111/j.1365-246X.2006.03171.x.

Krischer, L., Megies, T., Barsch, R., Beyreuther, M., Lecocq, T., Caudron, C., Wassermann, J., 2015. ObsPy: a bridge for seismology into the scientific python ecosystem. Comput. Sci. Discovery 8 (1), 014003. http://dx.doi.org/10.1088/1749-4699/8/1/014003.

Larose, E., Planès, T., Rossetto, V., Margerin, L., 2010. Locating a small change in a multiple scattering environment. Appl. Phys. Lett. 96, 1–3.

Lecocq, T., Caudron, C., Brenguier, F., 2014. MSNoise, a python package for monitoring seismic velocity changes using ambient seismic noise. Seismol. Res. Lett. 85 (3), 715–726. http://dx.doi.org/10.1785/0220130073.

Lees, J.M., 2007. Seismic tomography of magmatic systems. J. Volcanol. Geotherm. Res. 167 (1), 37–56.

Lénat, J.F., Bachèlery, P., Peltier, A., 2012. The interplay between collapse structures, hydrothermal systems, and magma intrusions: the case of the central area of Piton de la Fournaise volcano. Bull. Volcanol. 74 (2), 407–421.

Lesage, P., Reyes-Dávila, G., Arámbula-Mendoza, R., 2014. Large tectonic earthquakes induce sharp temporary decreases in seismic velocity in Volcán de Colima, Mexico. J. Geophys. Res. Solid Earth 119 (5), 4360–4376.

Lobkis, O.I., Weaver, R.L., 2001. On the emergence of the Green's function in the correlations of a diffuse field. J. Acoust. Soc. Am. 110 (6), 3011–3017.

Lyakhovsky, V., Hamiel, Y., Ampuero, J.P., Ben-Zion, Y., 2009. Non-linear damage rheology and wave resonance in rocks. Geophys. J. Int. 178 (2), 910–920.

Meier, U., Shapiro, N.M., Brenguier, F., 2010. Detecting seasonal variations in seismic velocities within Los Angeles basin from correlations of ambient seismic noise. Geophys. J. Int. 181 (2), 985–996.

Nakata, N., Chang, J.P., Lawrence, J.F., Boué, P., 2015. Body-wave extraction and tomography at Long Beach, California, with ambient-noise tomography. J. Geophys. Res. 120, 1159–1173. http://dx.doi.org/10.1002/2015JB01870.

Muco, B., 1995. The seasonality of Albanian earthquakes and cross correlation with rainfall. Phys. Earth Planet. Inter. 88, 285–291.

Nakata, N., Boué, P., Brenguier, F., Roux, P., Ferrazzini, V., Campillo, M., 2016. Body-and surface-wave reconstruction from seismic-noise correlations between arrays at Piton de la Fournaise volcano. Geophys. Res. Lett. 43, 1047–1054.

Obermann, A., Planès, T., Larose, E., Sens-Schönfelder, C., Campillo, M., 2013a. Depth sensitivity of seismic coda waves to velocity perturbations in an elastic heterogeneous medium. Geophys. J. Int. 194 (1), 372–382.

Obermann, A., Planès, T., Larose, E., Campillo, M., 2013b. Imaging pre- and co-eruptive structural changes of a volcano with ambient seismic noise. JGR 118, 1–10. http://dx.doi.org/10.1002/2013JB010399.

Obermann, A., Planès, T., Hadziioannou, C., Campillo, M., 2016. Lapse-time dependent coda wave depth sensitivity to local velocity perturbations in 3D heterogeneous elastic media (Submitted to GJI).

O'Connell, R.J., Budiansky, B., 1974. Seismic velocities in dry and saturated cracked solids. J. Geophys. Res. 79 (35), 5412–5426.

Pacheco, C., Snieder, R., 2005. Time-lapse travel time change of multiply scattered acoustic waves. J. Acoust. Soc. Am. 118, 1300–1310.

Patanè, D., Barberi, G., Cocina, O., De Gori, P., Chiarabba, C., 2006. Time-resolved seismic tomography detects magma intrusions at Mount Etna. Science 313 (5788), 821–823.

Peltier, A., Bachèlery, P., Staudacher, T., 2009. Magma transport and storage at Piton de La Fournaise (La Réunion) between 1972 and 2007: a review of geophysical and geochemical data. J. Volcanol. Geotherm. Res. 184 (1), 93–108.

Planès, T., Larose, E., Margerin, L., Rossetto, V., Sens-Schönfelder, C., 2014. Decorrelation and phase-shift of coda waves induced by local changes: multiple scattering approach and numerical validation. Waves Random Complex Media 2, 1–27.

Planès, T., Larose, E., Rossetto, V., Margerin, L., 2015. Imaging multiple local changes in heterogeneous media with diffuse waves. J. Acoust. Soc. Am. 137 (2), 660–667.

Poli, P., Campillo, M., Pedersen, H., Group, L.W., 2012. Body-wave imaging of Earth's mantle discontinuities from ambient seismic noise. Science 338, 1063–1065.

Poupinet, G., Ellsworth, W.L., Frechet, J., 1984. Monitoring velocity variations in the crust using earthquake doublets: an application to the Calaveras Fault, California. J. Geophys. Res. Solid Earth 89 (B7), 5719–5731 (1978–2012).

Ratdomopurbo, A., Poupinet, G., 1995. Monitoring a temporal change of seismic velocity in a volcano: application to the 1992 eruption of Mt. Merapi (Indonesia). Geophys. Res. Lett. 22 (7), 775–778.

Rhie, J., Romanowicz, B., 2004. Excitation of Earth's continuous free oscillations by atmosphere–ocean–seafloor coupling. Nature 431 (7008), 552–556.

Rivet, D., Brenguier, F., Clarke, D., Shapiro, N.M., Peltier, A., 2014. Long-term dynamics of Piton de la Fournaise volcano from 13 years of seismic velocity change measurements and GPS observations. J. Geophys. Res. Solid Earth 119 (10), 7654–7666.

Rivet, D., Brenguier, F., Cappa, F., 2015. Improved detection of preeruptive seismic velocity drops at the Piton de la Fournaise volcano. Geophys. Res. Lett. 42 (15), 6332–6339. http://dx.doi.org/10.1002/2015GL06483.

Rost, S., Thomas, C., 2002. Array seismology: methods and applications. Rev. Geophys. 40, 1008.

Roult, G., Peltier, A., Taisne, B., Staudacher, T., Ferrazzini, V., Di Muro, A., 2012. A new comprehensive classification of the Piton de la Fournaise activity spanning the 1985–2010 period. Search and analysis of short-term precursors from a broad-band seismological station. J. Volcanol. Geotherm. Res. 241, 78–104. http://dx.doi.org/10.1016/j.jvolgeores.2012.06.012.

Schimmel, M., Gallart, J., 2007. Frequency-dependent phase coherence for noise suppression in seismic array data. J. Geophys. Res. Solid Earth 112 (B4) (1978–2012).

Sens-Schönfelder, C., Wegler, U., 2006. Passive image interferometry and seasonal variations of seismic velocities at Merapi Volcano, Indonesia. Geophys. Res. Lett. 33 (21).

Sens-Schönfelder, C., Pomponi, E., Peltier, A., 2014. Dynamics of Piton de la Fournaise volcano observed by passive image interferometry with multiple references. J. Volcanol. Geotherm. Res. 276, 32–45.

Shalev, E., Lyakhovsky, V., 2013. The processes controlling damage zone propagation induced by wellbore fluid injection. Geophys. J. Int. 193 (1), 209–219.

Shapiro, S.A., 2003. Elastic piezosensitivity of porous and fractured rocks. Geophysics 68 (2), 482–486.

Shapiro, N.M., Campillo, M., 2004. Emergence of broadband Rayleigh waves from correlations of the ambient seismic noise. Geophys. Res. Lett. 31 (7).

Shapiro, N.M., Campillo, M., Stehly, L., Ritzwoller, M.H., 2005. High-resolution surface-wave tomography from ambient seismic noise. Science 307 (5715), 1615–1618.

Snieder, R., Grêt, A., Douma, H., Scales, J., 2002. Coda wave interferometry for estimating nonlinear behavior in seismic velocity. Science 295 (5563), 2253–2255.

Snieder, R., Hagerty, M., 2004. Monitoring change in volcanic interiors using coda wave interferometry: application to Arenal Volcano, Costa Rica. Geophys. Res. Lett. 31 (9).

Staudacher, T., Ferrazzini, V., Peltier, A., Kowalski, P., Boissier, P., Catherine, P., ... Massin, F., 2009. The April 2007 eruption and the Dolomieu crater collapse, two major events at Piton de la Fournaise (La Réunion Island, Indian Ocean). J. Volcanol. Geotherm. Res. 184 (1), 126–137.

Svejdar, V., Küchenhoff, H., Fahrmeir, L., Wassermann, J., 2011. External forcing of earthquake swarms at Alpine regions: example from a seismic meteorological network at Mt Hochstaufen SE-Bavaria. Non. Proc. Geophys. 18, 849–860. http://dx.doi.org/10.5194/npg-18-849-2011.

Taisne, B., Brenguier, F., Shapiro, N.M., Ferrazzini, V., 2011. Imaging the dynamics of magma propagation using radiated seismic intensity. Geophys. Res. Lett. 38 (4).

Talwani, P., Chen, L., Gahalaut, K., 2007. Seismogenic permeability, ks. J. Geophys. Res. 112, B07309. http://dx.doi.org/10.1029/2006JB004665.

Tarantola, A., Valette, B., 1982. Generalized non-linear inverse problems solved using the least-squares criterion. Rev. Geophys. 20 (2), 219–232.

Tsai, V.C., 2011. A model for seasonal changes in GPS positions and seismic wave speeds due to thermoelastic and hydrologic variations. J. Geophys. Res. Solid Earth 116 (B4) (1978–2012).

Weaver, R.L., Hadziioannou, C., Larose, E., Campillo, M., 2011. On the precision of noise correlation interferometry. Geophys. J. Int. 185 (3), 1384–1392.

Wegler, U., Lühr, B.G., Snieder, R., Ratdomopurbo, A., 2006. Increase of shear wave velocity before the 1998 eruption of Merapi volcano (Indonesia). Geophys. Res. Lett. 33 (9).

Yamamura, K., Sano, O., Utada, H., Takei, Y., Nakao, S., Fukao, Y., 2003. Long-term observation of in situ seismic velocity and attenuation. J. Geophys. Res. Solid Earth 108 (B6) (1978–2012).

Zinszner, B., Johnson, P.A., Rasolofosaon, P.N., 1997. Influence of change in physical state on elastic nonlinear response in rock: significance of effective pressure and water saturation. J. Geophys. Res. Solid Earth 102 (B4), 8105–8120 (1978–2012).